ACS APPLIED MATERIALS & INTERFACES

Research Article

www.acsami.org

Facile Fabrication of Robust Silk Nanofibril Films via Direct Dissolution of Silk in $CaCl_2$–Formic Acid Solution

Feng Zhang,[†,‡,∥] Xinran You,[†,∥] Hao Dou,[‡] Zhi Liu,[‡] Baoqi Zuo,*[,‡] and Xueguang Zhang*[,†,§]

[†]Medical College of Soochow University, Jiangsu Province Key Laboratory of Stem Cell Research, Soochow University, Suzhou 215123, China

[‡]National Engineering Laboratory for Modern Silk, College of Textile and Clothing Engineering, Soochow University, Suzhou 215123, China

[§]Institute of Clinical Immunology of Jiangsu Province, The First Affiliated Hospital of Soochow University, Suzhou, 215006, China

Supporting Information

ABSTRACT: In this study, we report for the first time a novel silk fibroin (SF) nanofibrous films with robust mechanical properties that was fabricated by directly dissolving silk in $CaCl_2$–formic acid solution. $CaCl_2$–FA dissolved silk rapidly at room temperature, and more importantly, it disintegrated silk into nanofibrils instead of separate molecules. The morphology of nanofibrils crucially depended on $CaCl_2$ concentrations, which resulted in different aggregation nanostructure in SF films. The SF film after drawing had maximum elastic modulus, ultimate tensile strength, and strain at break reaching 4 GPa, 106 MPa, and 29%, respectively, in dry state and 206 MPa, 28 MPa, and 188%, respectively, in wet state. Moreover, multiple yielding phenomena and substantially strain-hardening behavior was also observed in the stretched films, indicating the important role played by preparation method in regulating the mechanical properties of SF films. These exceptional and unique mechanical properties were suggested to be caused by preserving silk nanofibril during dissolution and stretching to align these nanofibrils. Furthermore, the SF films exhibit excellent biocompatibility, supporting marrow stromal cells adhesion and proliferation. The film preparation was facile, and the resulting SF films manifested enhanced mechanical properties, unique nanofibrous structures, and good biocompability.

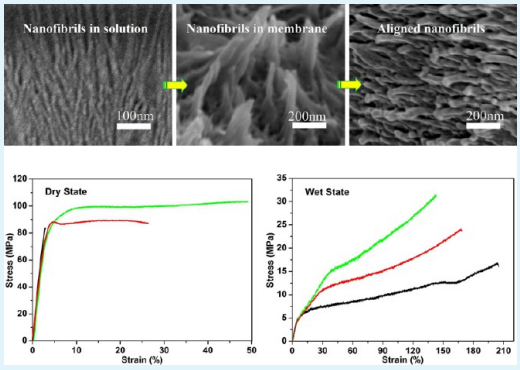

KEYWORDS: *silk fibroin, nanofibril, film, mechanical property, biocompatibility*

1. INTRODUCTION

Silk, known typically for its high tensile strength and great extensibility, is one of the toughest natural materials and outperforms most synthetic fibers.[1] The spinning process for silk is also environmentally friendly and energy saving. The superior physical and chemical properties and optimum spinning process make silk a promising alternative to high-performance synthetic fibers.[2] Despite the successful use as luxury fabric in its natural fiber form, silk is currently being explored to give multiple material formats, such as films, nanofibers, gels, and sponges, for high-technology applications.[3,4]

Silk fibroin (SF) film, as a main form of regenerated silk materials, has gained increased attention due to its unique physical, chemical, and biological properties, as well as its potential applications in the fields of tissue engineering, biosensing, electronic, optics, and photonics.[5,6] Generally, SF films can be successfully prepared from aqueous,[1] acidic,[7] ionic,[8] and N-methyl morpholine N-oxide (NMMO) solutions,[9] with the ability to control the morphology, crystalline state, nanostructure, mechanical properties, and degradability.[10−12] However, the regenerated SF films are brittle in a dry state[13] and have low strength and modulus in a wet state,[14] which will not satisfy the requirements of practical application. To cope with the shortcoming of regenerated silk materials, titanium,[15] carbon nanotubes,[16] graphene oxide,[17] and chitin[18] have been utilized as reinforcing agents or blending partners. In addition, uniaxial extension is also reported to be effective in improving the mechanical properties of regenerated silk fibers[19,20] and films[13,21] due to the increase of molecular and nanostructural orientation.

It is generally believed that the exceptional mechanical properties of silk is endowed by its complicated hierarchical structure that involving high molecular weight, β-sheet crystal structure, and fibrillar structure.[22,23] Recent study further confirms that fibrillar structure, especially at nanoscale, plays a critical role in defining the high performance of native silk.[24] Films built from nanofibrils have also shown extraordinary

Received: November 26, 2014
Accepted: January 20, 2015
Published: January 20, 2015

DOI: 10.1021/am508319h
ACS Appl. Mater. Interfaces 2015, 7, 3352−3361

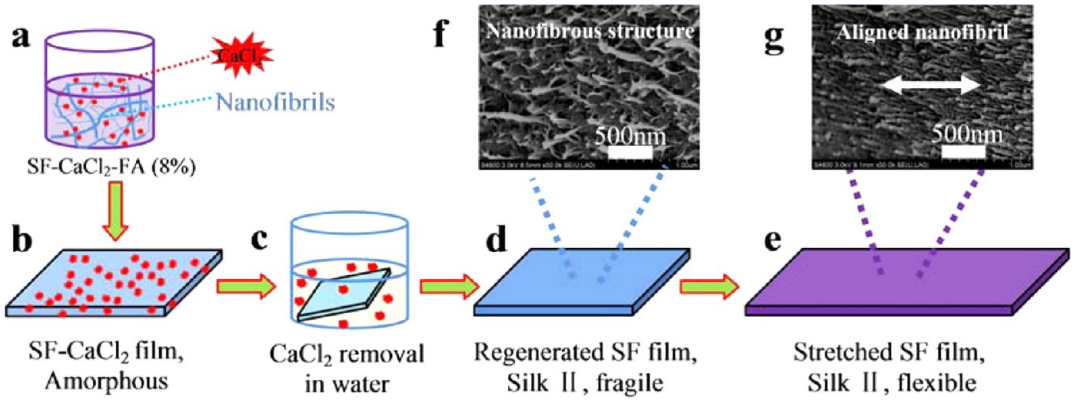

Figure 1. Schematic representation of SF films formation process: (a) dissolve degummed silk in $CaCl_2$–FA to form 8% SF solution; (b) cast on polystyrene Petri dishes to prepare SF film containing $CaCl_2$ after FA evaporation; (c) immerse in deionized water to remove $CaCl_2$ and residual FA; (d) dry at room ambient conditions to form regenerated SF film; (e) stretch in water to generate flexible SF film; (f) random arrangement of silk nanofibrils in SF film without stretch; and (g) aligned nanofibril in stretched SF films.

mechanical properties and advanced functionalities.[25] These nanofibrils can be self-assembled from peptides and proteins[26,27] and extracted from native materials such as chitin[28] and cellulose.[29,30] However, this important fibrillar structure is almost destroyed during the silk dissolution and regeneration process in a classical dissolving system, such as 9.3 M LiBr solution.[4] Although silk nanofibrils can be achieved through controlling self-assembly conditions,[26] and the resulting SF film displays flexibility to some extent,[13] the mechanical properties are still significantly inferior to those of natural silk fibers, likely due to the instability of these self-assembled nanofibrils.[31] Additionally, the time-consuming, multistep process of film preparation is another problem presented.[8] Our recent investigation revealed for the first time that silk could be directly dissolved in $CaCl_2$–formic acid (FA) solution while preserving its nanofibril structure,[32] allowing us to fabricate high-quality silk materials based on native silk nanofibrils in a rapid way.

In an attempt to gain a better understanding of the comprehensive effects of $CaCl_2$ concentrations on silk dissolution and of the structure and properties of SF film, and to explore high-performance SF films for use in biomedical applications, we employed four concentrations of $CaCl_2$ to dissolve silk and form SF films. Marrow stromal cells (MSCs) are capable of self-renewal and multilineage differentiation, presenting promising possibilities for cellular therapy and tissue engineering applications. Here, we employed MSCs to evaluate the cell biocompability of the above resulting SF films.

2. EXPERIMENTAL METHODS

2.1. Preparation of Silk Solutions. *Bombyx mori* silk fibroin was prepared according to the protocol as reported earlier.[32] Briefly, cocoons were boiled for 60 min in an aqueous solution of 0.05 wt % Na_2CO_3 and then rinsed thoroughly with distilled water to extract the sericin proteins. The degummed silk was then directly dissolved in $CaCl_2$–Formic acid (FA) at room temperature yielding an 8 wt % solution.

2.2. Film Formation. Regenerated silk fibroin films were prepared by pouring SF–$CaCl_2$–FA solution (8 wt %) in polystyrene Petri dishes (diameter 30 mm). The dishes containing silk solution were placed in an airing chamber to allow fast evaporation of formic acid within 24 h. The resulting SF films were directly immersed in water for 2 h to remove the $CaCl_2$ and residual formic acid and induce β-sheet structure. The SF films were air-dried and then placed in a vacuum-dryer for 24 h.

2.3. Scanning Electron Microscopy (SEM). The nanostructure of silk in $CaCl_2$–FA solution and the cross section of SF films were observed with S-4800 scanning electron microscopy (SEM, Hitachi, Tokyo, Japan) at 3 kV. The 8 wt % SF–$CaCl_2$–FA solution was diluted to 1 μg/mL by formic acid, and then dropped on silica plate for SEM imaging. The SF films were fractured in liquid nitrogen to avoid deformation. The specimens were sputter coated with gold prior to imaging.

2.4. Rheological Analysis. Rheological studies were run on a rheometer (AR2000, TA Instruments, America) with a 35 mm cone plate (Ti, 35/1°). The normal force applied on the sample during the lowering of the top plate was limited to 0.1 N. The shear rate was linearly increased from 0.01 to 5000 s^{-1} at 25 °C.

2.5. Fourier Transform Infrared (FTIR). FTIR spectra were obtained using a Magna spectrometer (NicoLET5700, America) in the spectral region of 400–4000 cm^{-1}. For each measurement, 32 scans were coded at a resolution of 4 cm^{-1}. The powdered SF films were pressed into potassium bromide (KBr) pellets prior to data collection.

2.6. X-ray Diffraction (XRD). XRD (X'PERT PRO MPD, PANalytical Company, The Netherlands) analyses were performed on SF films with Cu K radiation at 40 kV and 30 mA.

2.7. X-ray Photoelectron Spectroscopy (XPS). The surface chemical compositions of SF films were analyzed by SHIMADZU/KRATOS XPS to determine whether the $CaCl_2$ were removed completely from the as-cast SF films. FA as a volatile organic solvent was completely removed by evaporation and water rinse process as previous reports,[7,26] so its removal from silk films was not characterized. The incident angle of the X-rays was 90°, and the vacuum degree of the analysis chamber was less than or equal to 1×10^{-9} Pa. All the deviations of the binding energy in the XPS measurement were corrected by the carbon (C 1s) photoelectron emission signal occurring at 284.5 eV.

2.8. Contact Angles. The wettability of all SF films was determined by employing static contact angle measurements using degassed, ultrapurified water with a camera system coupled to a computer-assisted contour analysis program (OCA-50, DataPhysics Corp., Germany). A water droplet of 30 μL was placed on SF films. The contact angles were measured at five different areas for each sample to calculate means and SD.

2.9. Mechanical Testing. The mechanical data of SF films (10 × 50 mm, thickness of approximately 30 μm measured by micrometer) were tested using a universal testing machine (Instron 3365, Instron, Norwood, MA; gauge length, 20 mm; cross-head speed, 10 mm/min) equipped with a 100 N capacity load cell, at 25 ± 0.5 °C, 60 ± 5% relative humidity. For dry tests, samples were equilibrated in a constant temperature and humidity chamber for 24h at 25 ± 0.5 °C, 60 ± 5% relative humidity. For wet tests, samples were hydrated in 0.1 M phosphate-buffered saline (PBS) for 1 h to equilibrate prior to testing.

DOI: 10.1021/am508319h
ACS Appl. Mater. Interfaces 2015, 7, 3352–3361

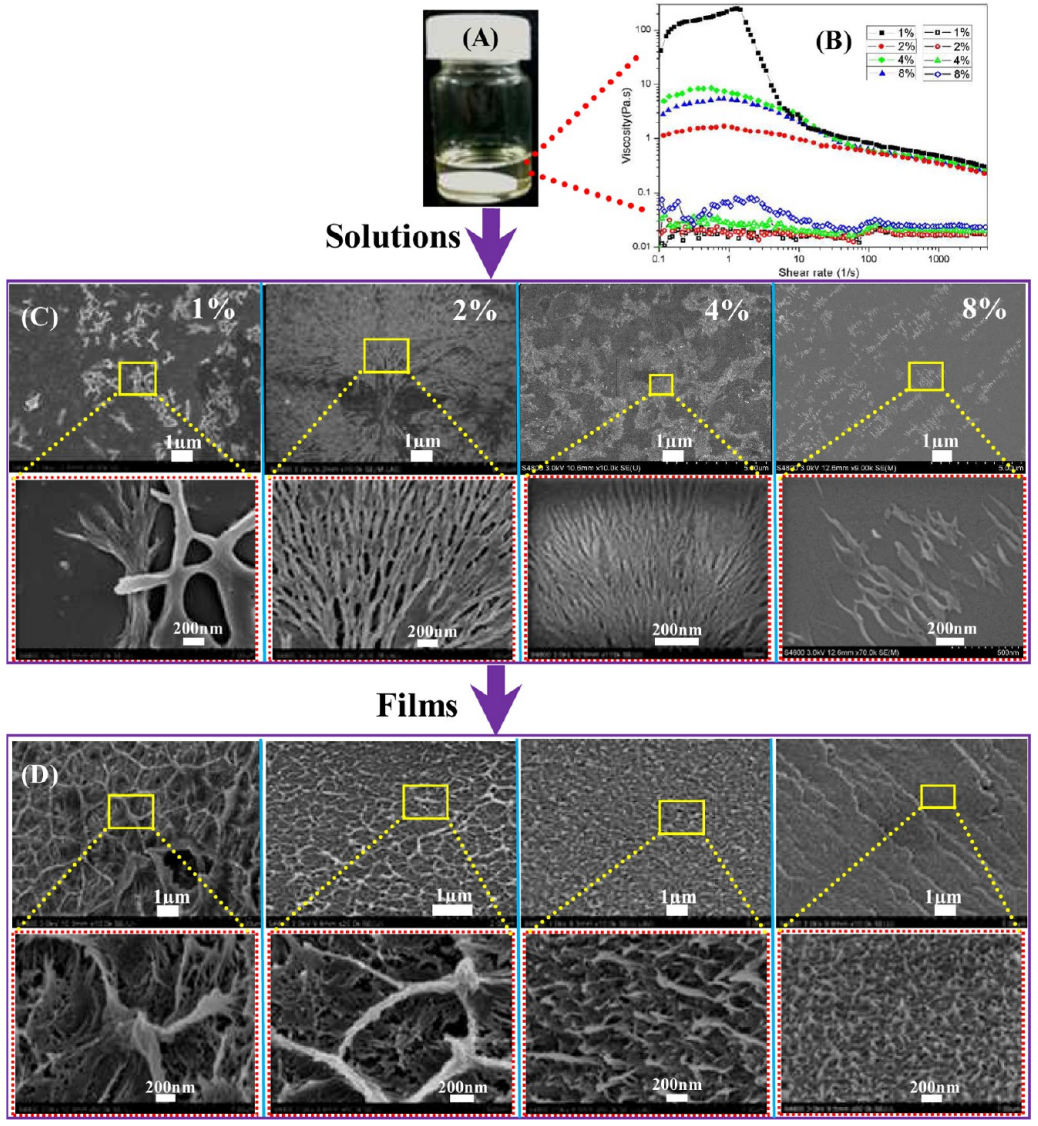

Figure 2. (A) Silk-$CaCl_2$–FA solution. (B) Viscosity shear rate profiles of silk solutions prepared by dissolving native silk fibroin (NSF, solid figures) and regenerated silk fibroin film[26] (RSF, hollow figures) in 1, 2, 4, and 8% $CaCl_2$–FA solution. (C) SEM images of silk–$CaCl_2$–FA solution showing varied nanofibrillar structure. (D) Fracture surface of SF films.

2.10. Cell Proliferation on Silk Fibroin Films. In this study, all experimental procedures involving animals were approved by the Animal Care and Use Committee of Soochow University. Marrow stromal cells (MSCs) were obtained from 5week old male Sprague–Dawley rats (150–200g) by flushing femurs and tibias with low-glucose Dulbecco's modified Eagle's medium (L-DMEM, Gibco, Carlsbad, CA) and they were cultivated in cultural media as described in our earlier report.[33] The nonadherent cells were discarded with the media changes, which were performed every 3 days. The adherent MSCs at 80–90% confluence was detached with 0.25% trypsin-EDTA (Sigma, San Francisco, CA) and subsequently to be cultured for next passages. MSCs at passage five were used for the experiments to avoid the effect of culture time on MSCs functions. MSCs were seeded at a density of 5.0×10^3 cells on the SF films prewetted with Dulbecco's modified Eagle's medium (DMEM). The cell culture medium was composed of L-DMEM with 10% fetal bovine serum (FBS, Gibco, Carlsbad, CA) and 1% penicillin–streptomycin, and was replaced first at 24 h, then every 72 h. MSCs grown on films were observed every day using inverted phase contrast microscope. MSCs proliferation was determined using MTT assay conducted as our previous report.[34]

2.11. Statistics. All experiments were performed with a minimum of $N = 3$ for each data point. Statistical analysis was performed by one-way analysis of variance (ANOVA). Difference were considered significant when $p \leq 0.05$.

3. RESULTS AND DISCUSSION

3.1. Nanostructure in Solution and Films. The fibril structure, which existed in native silk and spider silk, is specially tuned at the nanoscale by nature to achieve a combination of high strength and large elongation.[24] Our recent work found that $CaCl_2$–FA could dissolve silk easily while preserving its nanofibril structure under optimum degumming process.[32] In this study, regenerated SF films with nanofibrous structure were formed using this dissolving system, as shown in Figure 1. The resultant silk–$CaCl_2$–FA solutions were clear with a faint yellow color (Figure 2A), and show obviously different rheologies when compared to the same type solution prepared as the traditional method (Figure 2B).

It is known that rheological behavior is an indicator for protein aggregates structure in solution.[35] Therefore, we investigated the rheological behavior of SF solutions prepared by using $CaCl_2$–FA to dissolve native silk fibroin (NSF) and to

DOI: 10.1021/am508319h
ACS Appl. Mater. Interfaces 2015, 7, 3352–3361

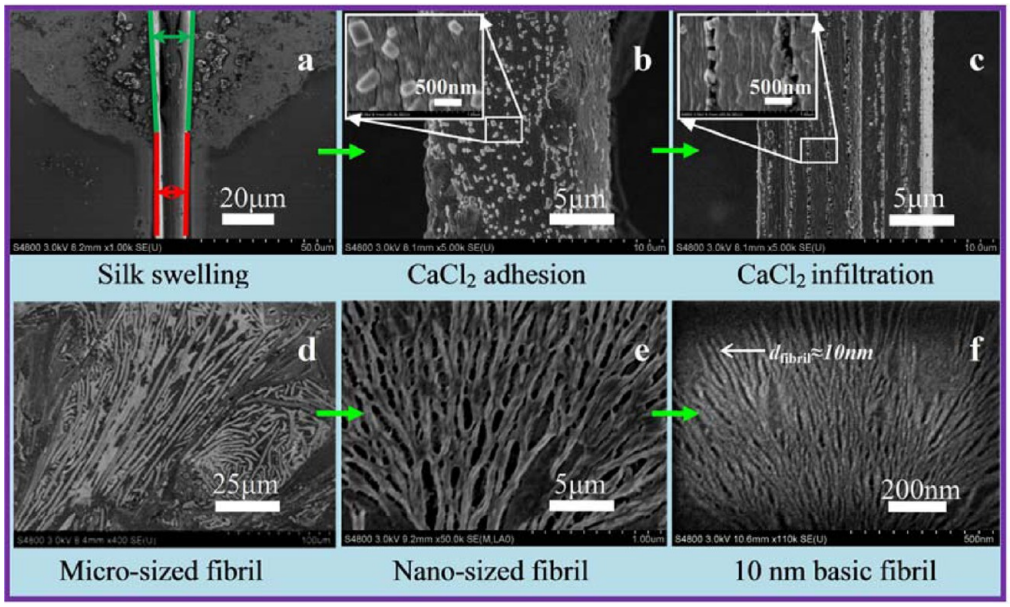

Figure 3. SEM micrographs showing the consecutive disassembly process of silk fibers: (a) $CaCl_2$−FA solution dropped onto the silk fibers caused degummed silk fiber swelling immediately; (b) $CaCl_2$ precipitation resulted small gaps on silk fiber; (c) big gaps appeared due to further $CaCl_2$ infiltration; (d) Silk disassembles into microsized fibrils; (e) microsized fibril disassembles into nanosized fibrils; and (f) nanosized fibril disassembles into 10 nm basic fibrils.

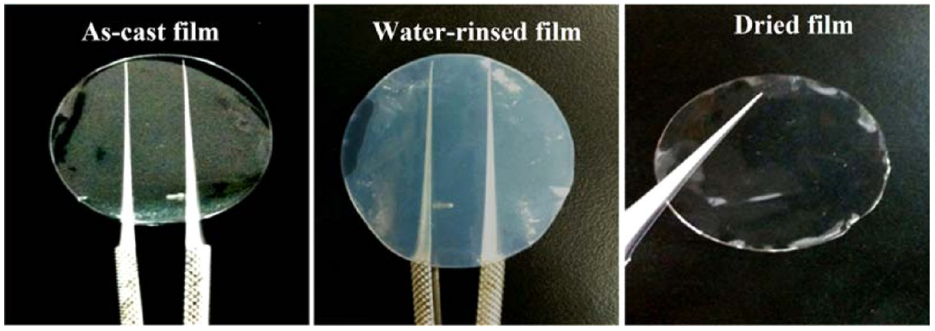

Figure 4. Images of SF films derived from $CaCl_2$−FA solution. Film thickness was around 30 μm.

dissolve regenerated silk fibroin films (RSF) derived from 9.3 M LiBr.[26] Obviously, the viscosity measurements over a range of shear rates confirmed the vast differences between these two solutions (Figure 2B). Over the range of shear rates tested, RSF solutions, flowed undisturbed, behaved like Newtonian fluids with significantly low viscosity independent of the $CaCl_2$−FA concentration, in agreement with previous finding.[36] In contrast, DSF solutions exhibited shear-thickening before the onset of shear-thinning with significantly higher viscosities which was similar to that of natural silk dopes.[37] The viscosity of 1% SF−$CaCl_2$−FA at lower shear rate was much higher that of others, and greatly decreased with the increase of shear rate, which was likely stem from the nanofibril aggregation or strong interaction between nanofibrils. The origin for the vast difference in the observed rheologies of RSF and DSF was in all probability due to the different protein nanostructure formed during the dissolving process.[26,38]

To clearly describe silk fibroin structure, we examined the solution behavior of these silk-$CaCl_2$−FA solution by SEM, and observed "fibrils" with size that varied depending on the concentration of $CaCl_2$ (Figure 2C). Figure 3 showed the dissolution process of silk in $CaCl_2$−FA solution, which started with fiber swelling. Then $CaCl_2$ precipitation and infiltration promoted silk fiber fibrillation. Finally, $CaCl_2$−FA gradually disintegrated macrofibers into microfiber, and then into nanofibrils. Once silk was dissolved in $CaCl_2$−FA solution, films were prepared by simple solution cast method. During this process, the solution concentration increased strongly, leading to nanofibril aggregation in the resultant films. It was clear that the films contained structural length scales on the mesoscale (Figure 2D). The inherent flexibility of nanoscale fibers led to tighter packing, less porous films, and transparency. These films were further immersed in water at room temperature to remove $CaCl_2$ (Figure 1c) and initiate structural transition to crystalline β-sheet. After being rinsed with water, films formed hydrogels due to film swelling and water adsorption.[11] Finally, these hydrogel films became completely transparent again after being dried (Figure 4). This behavior found in nanofibril-based films, insolubility in water, was completely different from those seen for SF films prepared from traditional solvents, such as aqueous LiBr solution[39] or ionic liquids.[8] The reason for this behavior was that water-stable nanofibril structure and interfibrillar bonding, such as hydrogen bonds, inhibited film dissolution. The nanofibril structure in SF films showed varied sizes corresponding to those observed in the silk−$CaCl_2$−FA solution. In addition, no specific

DOI: 10.1021/am508319h
ACS Appl. Mater. Interfaces 2015, 7, 3352−3361

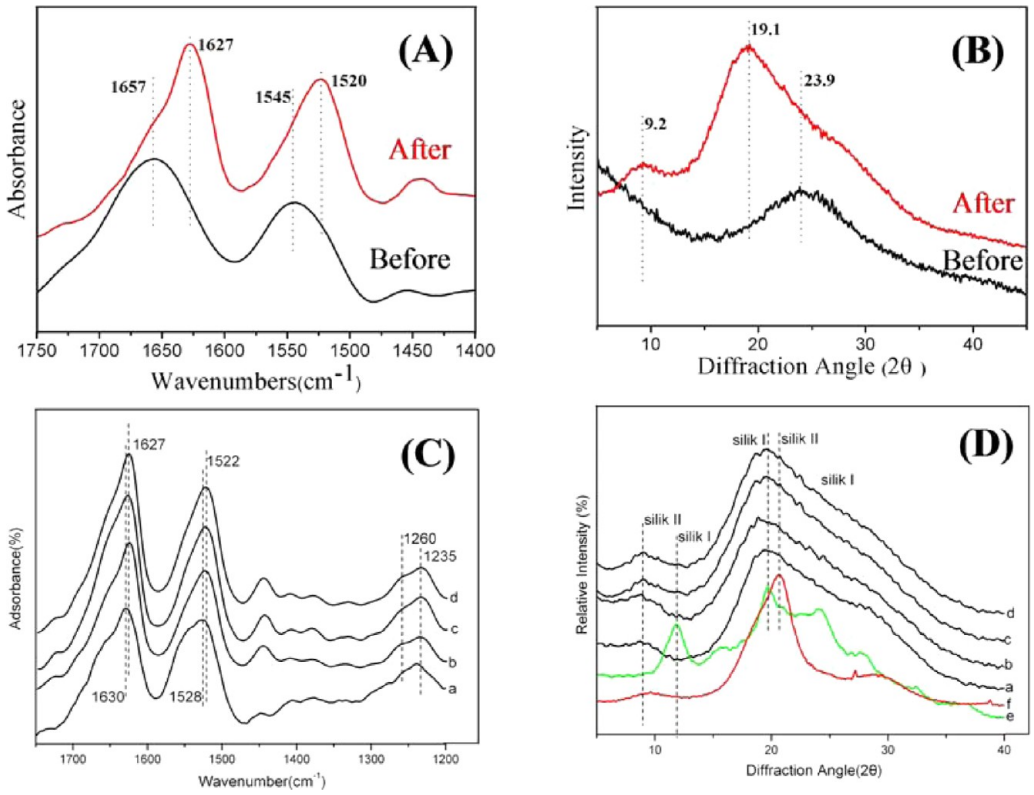

Figure 5. (A) FTIR and (B) XRD results demonstrated the structural transition of SF films derived from 4% $CaCl_2$–FA solution after water rinse. (C) FTIR and (D) XRD results of water rinsed SF films derived from (a) 1, (b) 2, (c) 4, and (d) 8% $CaCl_2$–FA solution, (e) SF films with silk I structure,[39] and (f) degummed silk with silk II structure.

nanostructure was found on the surface of these films, which all showed smooth characteristics except for the SF film derived from 1% $CaCl_2$–FA. Many residual fiber structures were observed on the film surface at 1% $CaCl_2$ concentration (Figure S1, Supporting Information), suggesting that the dissolution of silk was highly dependent on $CaCl_2$ concentration. Upon stretching, the randomly arranged nanofibrils in the SF films aligned along the stretch direction, which favored the increase of mechanical properties.[40] Therefore, SF films with tuned nanostructures could be generated through changing $CaCl_2$ concentrations.

3.2. Structure Characteristics. Changes in structure of the films during silk dissolution and film formation were detected by FTIR and XRD. The as-cast films initially showed a mainly amorphous structure (1545 cm^{-1}, amide II) with some α helix structure (1657 cm^{-1}, amide I; Figure 5A and Figure S2A, Supporting Information).[41] The XRD results further confirmed the mainly amorphous structure of SF films directly derived from $CaCl_2$–FA which was independent of $CaCl_2$ concentrations (Figure 5B and Figure S2B, Supporting Information). This, combined with the SEM results (Figure 2C), demonstrated that $CaCl_2$–FA disrupted the hydrogen bonds in the crystalline domains without collapse of nanofibril structure of the silk. Unlike the silk II structure observed in SF films prepared directly from FA, amorphous structure was formed in the SF films generated from $CaCl_2$–FA, indicating the role played by $CaCl_2$ in inhibiting silk crystallization during dry process in such dissolving system. In contrast, $CaCl_2$ could induce and promote conformational transition of silk from random coil to β-sheet in aqueous systems.[42] Although the main amorphous structure, these SF films were water-stable and could be immersed in water directly to remove $CaCl_2$ (Figures 1c and 4).

After being rinsed with water, the resultant SF films exhibited typically silk II structure (1627 cm^{-1}, amide I; 1522 cm^{-1}, amide II; Figure 5 A,C). The XRD data in Figure 5B,D further confirmed the structural transition from amorphous structure to crystalline β-sheet structure with peaks at 9.2 and 19.1°.[39] This structural transition was independent of $CaCl_2$ concentration (Figure 5C,D) though it plays an important role in regulating silk nanofibrillar structure (Figure 2). Compared with SF film with silk I structure and degummed silk with silk II structure, it was clear that the water-rinsed films exhibited a mixed silk I and silk II structure (Figure 5 D). Water annealing had been proved effective in inducing structural transition from amorphous structure to silk I, but not to silk II.[11] The mixed silk I and silk II structure was formed in the water-rinsed SF films, suggesting that the preserved nanofibrils might provide correct chain position favored protein crystallization.

Traditionally, the aqueous $CaCl_2$-silk solution was dialyzed against deionized water for about 3 days to generate pure silk fibroin scaffolds for biomedical applications.[4] In this study, we simply rinsed films in deionized water to remove unnecessary $CaCl_2$. XPS was used to estimate the surface composition of the SF films before and after water rinsing, as shown in Figure 6. The peak intensities of O_{1S}, N_{1S}, C_{1S} of silk fibroin at 530, 398, and 285 eV were observed in all the samples tested. The as-cast films initially exhibited the abundant existence of $CaCl_2$ with peak intensities at 108 eV (Ca 3p1/2), 160 eV (Ca 3s), 199 eV (Cl 2p), 350 eV (Ca 2p1/2), 439 eV (Ca 2s), and 490 eV (Ca (A)).[43] Upon rinse of the films to pure water, $CaCl_2$ was completely removed from the surface of films. In our previous

DOI: 10.1021/am508319h
ACS Appl. Mater. Interfaces 2015, 7, 3352–3361

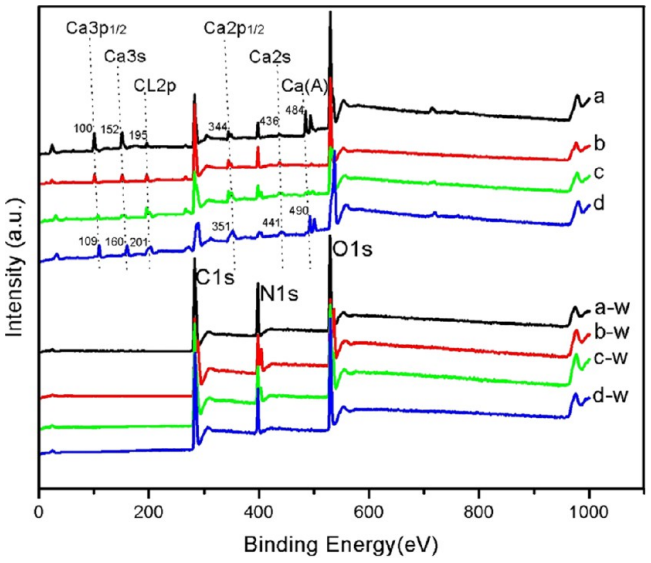

Figure 6. XPS spectra of SF film derived from (a) 1, (b) 2, (c) 4, and (d) 8% $CaCl_2$–FA solution. The letter "w" represents film after water rinse.

work, the electrospun mats derived from these water-rinsed films were also $CaCl_2$-free. Therefore, pure silk fibroin films without $CaCl_2$ could be prepared by simple water-rinse, although high weight ratios of $CaCl_2$ (~40%) were formed in the as-cast films.

3.3. Wettability of SF Films. The wettability of SF films derived from $CaCl_2$–FA was determined using static contact angle measurements. Contact angles for SF films increased from 79.5° to 85.1° as the decrease of $CaCl_2$ concentration from 10% to 1%. The results of contact angle test demonstrated that SF films prepared from $CaCl_2$–FA were more hydrophobic in terms of contact angle than that from water with amorphous, silk I, or silk II structure (Table1). The degummed silk fabric

Table 1. Comparison of Contact Angle Of SF Films Derived from $CaCl_2$–FA, and Films Derived from Aqueous LiBr Solution and Silk Fabric from the Literature

samples	contact angle (deg)[a]	ref
1%	85.1 ± 2.8[b]	this work
2%	83.2 ± 2.5[b]	this work
4%	82.1 ± 1.3[c]	this work
6%	82.3 ± 2.1[c]	this work
8%	82.0 ± 3.1[c]	this work
10%	79.5 ± 2.6	this work
amorphous film	51.4–67.3	1146,
silk I film	62.6 ± 1.8	11
silk II film	71.4 ± 1.5	11
silk fabric	88.9	44

[a]The significance of difference of silk films derived from 1, 2, 4, and 8% $CaCl_2$–FA from silk film derived from 10% $CaCl_2$–FA was obtained by one-way ANOVA analysis. [b]$p < 0.01$. [c]$p < 0.05$.

showed a high contact angle of 88.9°,[44] which was more hydrophobic than regenerated SF films. Besides, FA was a solvent that made the resulting SF films more hydrophobic as compared to other solvents, such as water, HFIP.[45] In this connection, the higher hydrophobic property of these films was likely due to the used solvent of formic acid and the higher content of β-sheet formed due to nanofibril preservation.[11,45] Therefore, SF films with low hydrophilicity could be directly prepared from $CaCl_2$–FA, and its hydrophobicity could be controlled by altering $CaCl_2$ concentration.

3.4. Mechanical Properties. Mechanical testing was performed on SF films derived from different $CaCl_2$ concentrations. The tensile testing curves are depicted in Figure 7, and all relevant data is summarized in Table 2. The

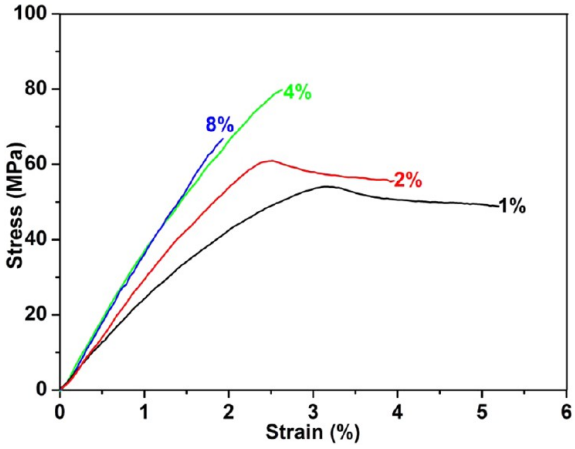

Figure 7. Stress–strain curve of SF films derived from 1, 2, 4, and 8% $CaCl_2$–FA solution.

effect of $CaCl_2$ concentration on the mechanical performance was evident in all samples. The SF films prepared from high $CaCl_2$ concentrations (≥4%) exhibited a linear stress–strain relationship and yielding hardly took place, whereas the SF films derived from low $CaCl_2$ concentrations (≤2%) displayed better flexibility and a distinct yield point, then remained almost constant in the yield region. The tensile testing curves showed stiffening, as seen by increased Young's modulus and tensile strength, and a decreased strain at break for higher $CaCl_2$ concentrations. The modulus, strength, and strain eventually reached the value of 4.1 GPa, 72.7 MPa, and 1.9% at 8% $CaCl_2$ concentration. The mechanical properties of these films derived from $CaCl_2$–FA were significantly superior to those of films with amorphous, silk I or silk II structure prepared by traditional methods (Table 2). The origin for this difference was likely due to the different fracture mechanism caused by different nanostructure. It had been widely reported that film with extraordinary mechanical properties was prepared using native cellulose and chitin nanofibrils.[18,28–30]

Although the improvement of mechanical properties was achieved due to the preserved nanofibril structure, the resulting SF films, reaching the highest strain value of about 5%, were still brittle in dry state. To overcome this shortcoming, the as-cast SF films were further stretched by the ratios of 50 and 100% with the aim to yield mechanically robust materials. Stretching silk fibers and films has been shown to increase both stress and strain by aligning molecular structure.[47] Upon physical stretching structural change, increased nanofibril orientation and molecular alignment were demonstrated (Figure 1 and Figure S3, Supporting Information), which significantly improved the mechanical properties in both dry and wet state.

SF films in dry state underwent a stretching-induced transition from predominantly linear elastic behavior to plastic deformation associated with a yield point, and followed by a fairly flat stress–strain region. It was caused by the lower

DOI: 10.1021/am508319h
ACS Appl. Mater. Interfaces 2015, 7, 3352–3361

Table 2. Overview of Mechanical Properties of SF Film Derived from $CaCl_2$–FA and Aqueous LiBr Solution

dry					
SF film	tensile modulus (GPa)	yield stress (MPa)	ultimate stress (MPa)	strain at break (%)	ref
1%	3.5 ± 0.3	53.2 ± 8.9	58.3 ± 9.2	5.7 ± 2.7	this work
2%	3.7 ± 0.2	60.1 ± 7.5	67.6 ± 8.7	4.3 ± 1.8	this work
4%	3.9 ± 0.5		81.4 ± 6.5	2.5 ± 0.9	this work
8%	4.1 ± 0.2		72.7 ± 5.3	1.9 ± 0.6	this work
50% stretch	3.0 ± 0.2	90.7 ± 2.0	88.7 ± 1.8	17.5 ± 6.8	this work
100% stretch	3.2 ± 0.1	99.0 ± 2.9	106.7 ± 2.5	28.9 ± 7.4	this work
silk I	2.7 ± 0.2	51.6 ± 5.2	48.5 ± 4.3	3.1 ± 0.5	this work
as cast	3.9 ± 0.7		47.2 ± 6.4	1.9 ± 0.7	11
methanol-treated	3.5 ± 0.9		58.8 ± 16.7	2.1 ± 0.4	11
ultrathin	6–8		100	0.5–3.0	12
wet					
SF film	tensile modulus (MPa)	yield stress (MPa)	ultimate stress (MPa)	strain at break (%)	ref
4%	206.8 ± 16.6	7.5 ± 0.7	17.7 ± 2.3	188.3 ± 16.3	this work
50% stretch	175.2 ± 19.8	5.2 ± 0.1 12.0 ± 1.1	23.5 ± 4.5	150.1 ± 20.1	this work
100% stretch	148.9 ± 15.2	5.3 ± 0.4 14.9 ± 2.8	27.8 ± 4.0	134.8 ± 9.1	this work
silk I	19.1 ± 0.2	1.8 ± 0.2	3.4 ± 0.3	145.2 ± 26.8	this work
silk II	40.2 ± 3.3	3.2 ± 0.3	5.1 ± 0.4	52 ± 4.9	this work
water annealing	22.0 ± 1.5	2.0 ± 0.1	3.6 ± 0.8	136 ± 48	14
methanol-treated	18.7 ± 7.0	2.3 ± 0.4	4.0 ± 1.0	149 ± 45	14

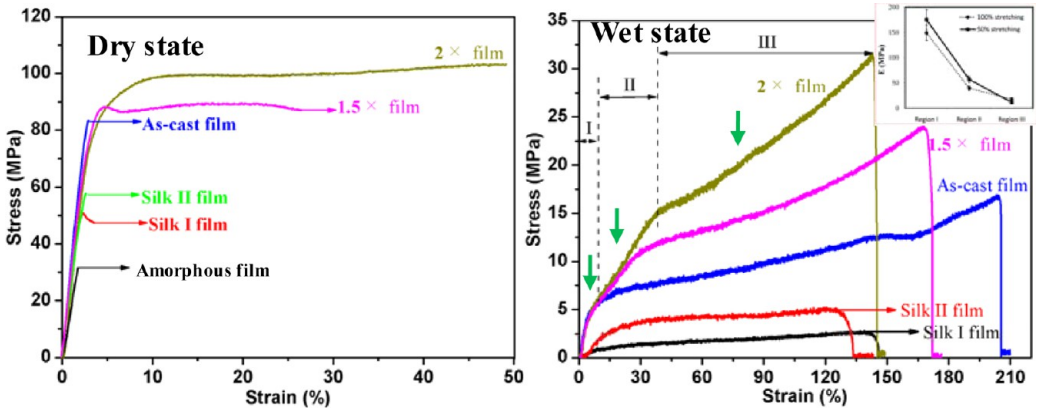

Figure 8. Stress–strain curves of SF films derived from 4% $CaCl_2$–FA solution with draw ratios of 1.5 and 2, and amorphous film (as-cast), silk I film (slow-drying), and silk II (methanol treatment) films derived from aqueous LiBr solution.

nanofibrillar friction at higher orientation distribution to allow for slippage. SEM imaging demonstrated that SF films displayed internal fibrillar alignment (Figure 1) consistent with the observations of this morphology in native silk fibers.[32] In addition, increasing drawing ratio led to higher breaking stress, yield stress, and elongation, but lower Young's modulus.

SF films in wet state displayed significantly lower Young's modulus and yield point and, most importantly, a much higher elongation due to the water plasticization. The effect of water absorption on the drawing behavior of SF films were seen in two respects. On one hand, water molecules adsorbed on the nanofibril and fibroin molecules surface and acted as competitive agent for interfibrillar and intermolecules hydrogen bonding, thus making the interfibrillar slippage and molecular rearrangement easier. On the other hand, water molecules were expected to act as lubricants and contributed to the molecular alignment. It could be seen that SF film was relatively weak and behaved like rubber, whereas the stretched film displayed significantly improved breaking strength. Interestingly, unlike films in the dry state, in which stretching significantly increased the strain at break of SF films, for films in the wet state, stretching decreased their extensibility and decreased with the drawing ratio. It was speculated that the extensibility of SF film was attributed to random arrangement of nanofibril and fibroin chains, which were aligned during the stretching in the wet state. The aligned nanofibril and fibroin chains favored film extensibility in the dry state but restricted this property in the wet state. A striking and unexpected multiple yielding phenomena was also found in the stretched SF films independently of draw ratios, which divided the stress–strain curves into three distinct region. The initial modulus of these three regions decreased with strain (inset, Figure 8). Region I, the films demonstrated an almost purely linear elastic behavior, in which the stress increased rapidly with strain. The identification of two additional regions (Regions II and III) featured a unique drawing behavior of increasing strain hardening (upturn in stress–strain curves, highlighted by green arrows). Stretching and hydration in water were required to observe such unique behavior, in agreement with the mechanical test on sericin and cellulose film.[25,48] The results demonstrated the important role played by dissolving system

DOI: 10.1021/am508319h
ACS Appl. Mater. Interfaces 2015, 7, 3352–3361

and stretching treatment in regulating the mechanical properties of SF films.

3.5. Cell Compatibility. To evaluate the film properties related to biological response, marrow stromal cells (MSCs) were cultured on SF films cast on the bottom of 24 well nontissue-culture-treated plates. Figure 9 showed the inverted phase contrast microscope images of MSCs grown in SF films. The MSCs adhered to the film surface, and their spreading and proliferation were realized. The cell seeded on SF films exhibited a biological behavior similar to that on control. MTT results further revealed a linear increase in the number of MSCs on SF films and control from day 2 to day 6 (Figure 10). However, the SF films derived from 1% $CaCl_2$–FA solution demonstrated lower cell number on days 4 and 6, which was likely due to the undissolved fibers preventing cell attachment, as observed in Figure 9. The cell attachment, spread and proliferation observed on SF films demonstrated a similar cell responses to that observed with commonly used tissue-cultured-treated plates, suggesting that this film was suitable scaffolds for use in biomedical applications.

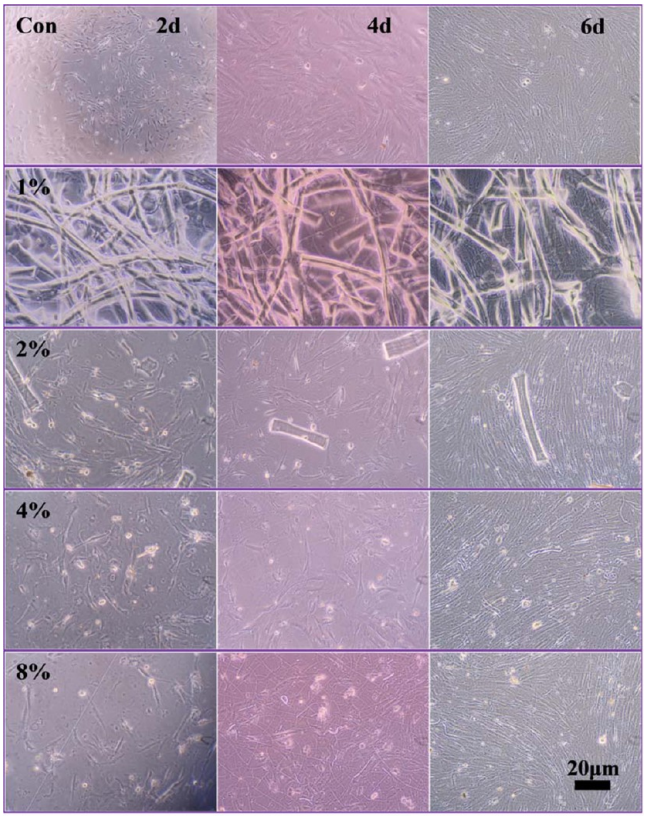

Figure 9. Attachment and proliferation of MSCs growing on SF films derived from $CaCl_2$–FA solution.

4. CONCLUSIONS

In summary, we demonstrated a facile method to fabricate silk fibroin films with nanofibrous structure, enhanced mechanical properties in dry and wet states, and good biocompatibility by using $CaCl_2$–formic acid solution as dissolving solvent and water as rinsing solvent. $CaCl_2$–FA could dissolve only interfibrillar parts consisting mainly of amorphous regions and could not dissolve highly crystalline nano- or microfibrils in raw degummed fiber. At that time, $CaCl_2$–FA was sorbed into nanofibrils and swelled the fibrils. Consequently, the β-sheet in nanofibrils was temporarily transformed to random coils without collapse of nanofibril structure. These findings offered a new perspective for the fabrication of biocompatible silk materials with nanofibrous structures and exceptional mechanical properties based on these nanofibrils, and the novel materials had potential applications in high-tech areas.

■ ASSOCIATED CONTENT

Supporting Information

Surface SEM images, FTIR and XRD spectra of the as-cast silk fibroin film, and Raman spectra of the stretched silk fibroin film. This material is available free of charge via the Internet at http://pubs.acs.org.

■ AUTHOR INFORMATION

Corresponding Authors

*Tel.: +86 512 65732002. E-mail: xueguangzh@126.com.
*Tel.: +86 512 67061157. E-mail: bqzuo@suda.edu.cn.

Author Contributions

‖These authors contributed equally to this work.

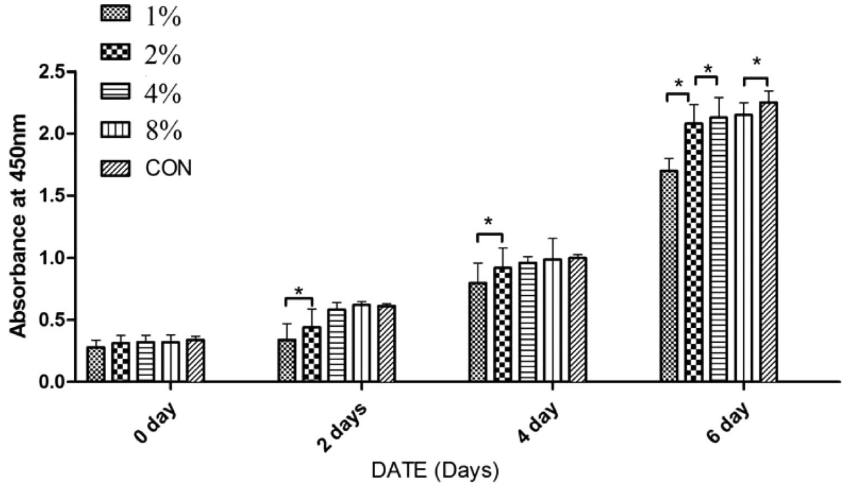

Figure 10. MTT assay for growth of MSCs on SF films derived from $CaCl_2$–FA solution. Error bars represent standard deviation with $N = 3$ ($p \leq 0.05$, where p = probability).

DOI: 10.1021/am508319h
ACS Appl. Mater. Interfaces 2015, 7, 3352–3361

Notes

The authors declare no competing financial interest.

■ ACKNOWLEDGMENTS

This project was supported by the Priority Academic Program Development of Jiangsu Higher Education Institutions (PAPD), Defense Basic Research Projects (B3820133001), the 973 Plan Research Special Subject (2012CB22302), the National Natural Science Foundation of China (51403142, 81472920), the Natural Science Foundation of Jiangsu Province (BK20141207), and the Research and Innovation Project for College Graduates of Jiangsu Province (CXZZ13_0817).

■ REFERENCES

(1) Karve, K. A.; Gil, E. S.; McCarthy, S. P.; Kaplan, D. L. Effect of β-sheet Crystalline Content on Mass Transfer in Silk Films. *J. Membr. Sci.* **2011**, *383*, 44−49.
(2) Holland, C.; Vollrath, F.; Ryan, A. J.; Mykhaylyk, O. O. Silk and Synthetic Polymers: Reconciling 100 Degrees of Separation. *Adv. Mater.* **2012**, *24*, 105−109.
(3) Omenetto, F. G.; Kaplan, D. L. New Opportunities for an Ancient Material. *Science* **2010**, *329*, 528−531.
(4) Rockwood, D. N.; Preda, R. C.; Yücel, T.; Wang, X.; Lovett, M. L.; Kaplan, D. L. Materials Fabrication from *Bombyx mori* Silk Fibroin. *Nat. Protoc.* **2011**, *6*, 1612−1631.
(5) Hu, T.; Kaplan, D. L.; Omenetto, F. G. Silk Materials−A Road to Sustainable High Technology. *Adv. Mater.* **2012**, *24*, 2824−2837.
(6) Perry, H.; Gopinath, A.; Kaplan, D. L.; Negro, L. D.; Omenetto, F. G. Nano- and Micropatterning of Optically Transparent, Mechanically Robust, Biocompatible Silk Fibroin Films. *Adv. Mater.* **2008**, *20*, 3070−3072.
(7) Rajkhowa, R.; Levin, B.; Redmond, S. L.; Li, L. H.; Wang, L.; Kanwar, J. R.; Atlas, M. D.; Wang, X. Structure and Properties of Biomedical Films Prepared from Aqueous and Acidic Silk Fibroin Solutions. *J. Biomed. Mater. Res., Part A* **2011**, *97A*, 37−45.
(8) Phillips, D. M.; Drummy, L. F.; Conrady, D. G.; Fox, D. M.; Naik, R. R.; Stone, M. O.; Trulove, P. C.; De Long, H. C.; Mantz, R. A. Dissolution and Regeneration of *Bombyx Mori* Silk Fibroin Using Ionic Liquids. *J. Am. Chem. Soc.* **2004**, *126*, 14350−14351.
(9) Freddi, G.; Pessina, G.; Tsukada, M. Swelling and Dissolution of Silk Fibroin (*Bombyx Mori*) in N-methyl Morpholine N-oxide. *Int. J. Biol. Macromol.* **1999**, *24*, 251−263.
(10) Lu, Q.; Zhang, B.; Li, M.; Zuo, B.; Kaplan, D. L.; Huang, Y.; Zhu, H. Degradation Mechanism and Control of Silk Fibroin. *Biomacromolecules* **2011**, *12*, 1080−1086.
(11) Jin, H. J.; Park, J.; Karageorgiou, V.; Kim, U.; Valluzzi, R.; Cebe, P.; Kaplan, D. L. Water-Stable Silk Films with Reduced β-sheet Content. *Adv. Funct. Mater.* **2005**, *15*, 1241−1247.
(12) Jiang, C.; Wang, X.; Gunawidjaja, R.; Lin, Y. H.; Gupta, M. K.; Kaplan, D. L.; Naik, R. R.; Tsukruk, V. V. Mechanical Properties of Robust Ultrathin Silk Fibroin Films. *Adv. Funct. Mater.* **2007**, *17*, 2229−2237.
(13) Zhang, C.; Song, D.; Lu, Q.; Hu, X.; Kaplan, D. L.; Zhu, H. Flexibility Regeneration of Silk Fibroin in Vitro. *Biomacromolecues* **2012**, *13*, 2148−2153.
(14) Lawrence, B. D.; Wharram, S.; Kluge, J. A.; Leisk, G. G.; Omenetto, F. G.; Rosenblatt, M. I.; Kaplan, D. L. Effect of Hydration on Silk Film Material Properties. *Macromol. Biosci.* **2010**, *10*, 393−403.
(15) Lee, S. M.; Pippel, E.; Gösele, U.; Dresbach, C.; Qin, Y.; Chandran, C. V.; Bräuniger, T.; Hause, G.; Knez, M. Greatly Increased Toughness of Infiltrated Spider Silk. *Science* **2009**, *324*, 488−492.
(16) Cho, S. Y.; Yun, Y. S.; Kim, E. S.; Kim, M. S.; Jin, H. J. Stem Cell Response to Multiwalled Carbon Nanotube-Incorporated Regenerated Silk Fibroin Films. *J. Nanosci. Nanotechnol.* **2011**, *11*, 801−805.
(17) Hu, K.; Gupta, M. K.; Kulkarni, D. D.; Tsukruk, V. V. Ultra-Robust Graphene Oxide−Silk Fibroin Nanocomposite Membranes. *Adv. Mater.* **2013**, *25*, 2301−2307.
(18) Jin, J.; Hassanzadeh, P.; Perotto, G.; Sun, W.; Brenckle, M. A.; Kaplan, D. L.; Omenetto, F. G.; Rolandi, M. A Biomimetic Composite from Solution Self-Assembly of Chitin Nanofibers in a Silk Fibroin Matrix. *Adv. Mater.* **2013**, *25*, 4482−4487.
(19) Sun, M.; Zhang, Y.; Zhao, Y.; Shao, H.; Hu, X. The Structure−Property Relationships of Artificial Silk Fabricated by Dry-Spinning Process. *J. Mater. Chem.* **2012**, *22*, 18372−18379.
(20) Zhou, G.; Shao, Z.; Knight, D. P.; Yan, J.; Chen, X. Silk Fibers Extruded Artificially from Aqueous Solutions of Regenerated *Bombyx mori* Silk Fibroin are Tougher than Their Natural Counterparts. *Adv. Mater.* **2009**, *21*, 366−370.
(21) Yin, J.; Chen, E.; Porter, D.; Shao, Z. Enhancing the Toughness of Regenerated Silk Fibroin Film through Uniaxial Extension. *Biomacromolecules* **2010**, *11*, 2890−2895.
(22) Vollrath, F.; Knight, D. P. Liquid Crystalline Spinning of Spider Silk. *Nature* **2001**, *410*, 541−548.
(23) Keten, S.; Xu, Z.; Ihle, B.; Buehler, M. J. Nanoconfinement Controls Stiffness, Strength and Mechanical Toughness of Beta-Sheet. *Nat. Mater.* **2010**, *9*, 359−67.
(24) Giesa, T.; Arslan, M.; Pugno, N. M.; Buehler, M. J. Nanoconfinement of Spider Silk Fibrils Begets Superior Strength, Extensibility, and Toughness. *Nano Lett.* **2011**, *11*, 5038−46.
(25) Benítez, A. J.; Torres-Rendon, J.; Poutanen, M.; Walther, A. Humidity and Multiscale Structure Govern Mechanical Properties and Deformation Modes in Films of Native Cellulose Nanofibrils. *Biomacromolecules* **2013**, *14*, 4497−4506.
(26) Zhang, F.; Zuo, B.; Fan, Z.; Xie, Z.; Lu, Q.; Zhang, X.; Kaplan, D. L. Mechanisms and Control of Silk-based Electrospinning. *Biomacromolecules* **2012**, *13*, 798−804.
(27) Hartgerink, J. D.; Beniash, E.; Stupp, S. I. Self-Assembly and Mineralization of Peptide−Amphiphile Nanofibers. *Science* **2001**, *294*, 1684−1688.
(28) Ifuku, S.; Saimoto, H. Chitin Nanofibers: Preparations, Modifications, and Applications. *Nanoscale* **2012**, *4*, 3308−3318.
(29) Moon, R. J.; Martini, A.; Nairn, J.; Simonsen, J.; Youngblood, J. Cellulose Nanomaterials Review: Structure, Properties and Nanocomposites. *Chem. Soc. Rev.* **2011**, *40*, 3941−3994.
(30) Klemm, D.; Kramer, F.; Moritz, S.; LindstrÖm, T.; Ankerfors, M.; Gray, D.; Dorris, A. Nanocelluloses: A New Family of Nature-based Materials. *Angew. Chem., Int. Ed.* **2011**, *50*, 5438−5466.
(31) Bai, S.; Zhang, X.; Lu, Q.; Sheng, W.; Liu, L.; Dong, B.; Kaplan, D. L.; Zhu, H. Reversible Hydrogel−Solution System of Silk with High Beta-sheet Content. *Biomacromolecules* **2014**, *15*, 3044−3051.
(32) Zhang, F.; Lu, Q.; Ming, J.; Dou, H.; Liu, Z.; Zuo, B.; Qin, M.; Li, F.; Kaplan, D. L.; Zhang, X. Silk Dissolution and Regeneration at the Nanofibril Scale. *J. Mater. Chem. B* **2014**, *2*, 3879−3885.
(33) Qua, J.; Zhou, D.; Xu, X.; Zhang, F.; He, L.; Ye, R.; Zhu, Z.; Zuo, B.; Zhang, H. Optimization of Electrospun TSF Nanofiber Alignment and Diameter to Promote Growth and Migration of Mesenchymal Stem Cells. *Appl. Surf. Sci.* **2012**, *261*, 320−326.
(34) Shen, Y.; Qian, Y.; Zhang, H.; Zuo, B.; Lu, Z.; Fan, Z.; Zhang, P.; Zhang, F.; Zhou, C. Guidance of Olfactory Ensheathing Cell Growth and Migration on Electrospun Silk Fibroin Scaffolds. *Cell Transplant.* **2010**, *19*, 147−57.
(35) Rammensee, S.; Slotta, U.; Scheibel, T.; Bausch, A. R. Assembly Mechanism of Recombinant Spider Silk Proteins. *Proc. Natl. Acad. Sci. U.S.A.* **2008**, *105*, 6590−6595.
(36) Holland, C.; Terry, A. E.; Porter, D.; Vollrath, F. Natural and Unnatural Silks. *Polymer* **2007**, *48*, 3388−3392.
(37) Holland, C.; Terry, A. E.; Porter, D.; Vollrath, F. Comparing the Rheology of Native Spider and Silkworm Spinning Dope. *Nat. Mater.* **2006**, *5*, 870−874.
(38) Bai, S.; Liu, S.; Zhang, C.; Xu, W.; Lu, Q.; Han, H.; Kaplan, D. L.; Zhu, H. Controllable Transition of Silk Fibroin Nanostructures: An Insight into in Vitro Silk Self-Assembly Process. *Acta Biomater.* **2013**, *9*, 7806−7813.

DOI: 10.1021/am508319h
ACS Appl. Mater. Interfaces 2015, 7, 3352−3361

(39) Lu, Q.; Hu, X.; Wang, X.; Kluge, J. A.; Lu, S.; Cebe, P.; Kaplan, D. L. Water-insoluble Silk Films with Silk I Structure. *Acta Biomater.* **2010**, *6*, 1380−1387.
(40) Jin, H. J.; Kaplan, D. L. Mechanism of Silk Processing in Insects and Spiders. *Nature* **2003**, *424*, 1057−1061.
(41) Hu, X.; Kaplan, D.; Cebe, P. Determining Beta-sheet Crystallinity in Fibrous Proteins by Thermal Analysis and Infrared Spectroscopy. *Macromolecules* **2006**, *39*, 6161−6170.
(42) Kim, U. J.; Park, J.; Li, C.; Jin, H. J.; Valluzzi, R.; Kaplan, D. L. Structure and Properties of Silk Hydrogels. *Biomacromolecules* **2004**, *5*, 786−792.
(43) Liu, Z.; Zhang, F.; Ming, J.; Bie, S.; Li, J.; Zuo, B. Preparation of Electrospun Silk Fibroin Nanofibers from Solutions Containing Native Silk Fibrils. *J. Appl. Polym. Sci.* **2015**, *132*, DOI: 10.1002/app.41236.
(44) Li, S.; Xing, T.; Li, Z.; Chen, G. Structure and Properties of Silk Grafted with Acrylate Fluoride Monomers by ATRP. *Appl. Surf. Sci.* **2013**, *268*, 92−97.
(45) Seib, F. P.; Maitz, M. F.; Hu, X.; Werner, C.; Kaplan, D. L. Impact of Processing Parameters on the Haemocompatibility of *Bombyx Mori* Silk Films. *Biomaterials* **2012**, *33*, 1017−1023.
(46) Bhattacharjee, M.; Schultz-Thater, E.; Trella, E.; Miot, S.; Das, S.; Loparic, M.; Ray, A. R.; Martin, I.; Spagnoli, G. C.; Ghosh, S. The Role of 3D Structure and Protein Conformation on the Innate and Adaptive Immune Response to Silk-based Biomaterials. *Biomaterials* **2013**, *34*, 8161−8171.
(47) Tucker, C. L.; Jones, J. A.; Bringhurst, H. N.; Copeland, C. G.; Addison, J. B.; Weber, W. S.; Mou, Q.; Yarger, J. L.; Lewis, R. V. Mechanical and Physical Properties of Recombinant Spider Silk Films using Organic and Aqueous Solvents. *Biomacromolecues* **2014**, *15*, 3158−3170.
(48) Kameda, T.; Kojima, K.; Togawa, E.; Sezutsu, H.; Zhang, Q.; Teramoto, H.; Tamada, Y. Drawing-Induced Changes in Morphology and Mechanical Properties of Hornet Silk Gel Films. *Biomacromolecules* **2010**, *11*, 1009−1018.

DOI: 10.1021/am508319h
ACS Appl. Mater. Interfaces 2015, 7, 3352−3361